Modulation-instability analysis of axial-azimuthal modes in surface nanoscale axial photonic microresonators

Alena Yu. Kolesnikova* and Ilya D. Vatnik
Physics Department, Novosibirsk State University, 2 Pirogova Street, Novosibirsk 630090, Russia

(Received 16 January 2024; accepted 1 May 2024; published 17 May 2024)

We study the initiation of primary comb generation in surface nanoscale axial photonic (SNAP) microcavities within the framework of modulation instability theory. In such cylindrical microcavities, the whispering gallery modes exhibit different effective volumes as well as varying overlap integrals with the excitation field, which poses a challenge to the process of nonlinear mode generation. We derive the threshold power for the nonlinear generation and find it considerably diverse for modes with different sideband numbers. We also suggest special dispersion control, effectively reducing the threshold and simplifying the generation in cylindrical cavities.

DOI: 10.1103/PhysRevA.109.053520

I. INTRODUCTION

The surface nanoscale axial photonics (SNAP) platform is aimed at creating cylindrical microcavities of whispering gallery modes made of standard optical fiber [1]. As with the other types of microresonators with small mode volumes and low losses, SNAP cavities are eligible for consideration for Kerr optical frequency comb generation under continuous-wave laser pumping.

Owing to a tiny disturbance of the cylinder radius that can be precisely introduced to the fiber cladding [2], SNAP mode structure possesses two sets of almost equidistant modes with extremely different free spectral ranges (FSRs), which may undergo four-wave mixing due to Kerr nonlinearity [3]. Firstly, there is a set of modes with one radial and one axial number, having the same field distribution along the cylinder axis but different azimuthal numbers m [see Fig. 1(a)]. The FSR is determined by the fiber radius and has a typical value on the order of 500 GHz.

The second set includes modes with the same azimuthal and radial numbers but different axial quantum numbers q. Axial distributions depend on the shape of the effective radius variation and are determined from the Schrödinger equation [1]. In the particular case of the parabolic shape of the variations, the axial mode series becomes equidistant [see Fig. 1(b)]. The FSR is regulated by the width and height of the radius variation and can be squeezed down to $\leqslant$100 MHz [4]. Thus, the SNAP system in principle can be used to generate optical frequency combs with both high and low repetition rates [3,5].

At the same time, there are peculiarities complicating the observation of Kerr nonlinear mode generation in SNAP microcavities, possibly explaining the absence of experimental evidence of nonlinear interactions in such cavities. This is likely due to the larger volume of SNAP cavity modes compared with other microcavities as well as the different mode volumes for different axial modes that are expected to increase the nonlinear generation threshold.

The arising of the primary comb as a result of degenerate four-wave mixing is well described within the theory of modulation instability (MI). Theories of MI in microcavities with an equidistant set of azimuthal modes have already been proposed previously [6–11]. The theories were successfully applied to the study of nonlinear generation for various types of microcavities, for example, ring GaP microresonators [12], crystalline MgF_2 microresonators [8,13], planar SiN microresonators on a photonic chip [14], Si_3N_4 microring resonators [8], microresonators with backscattering [15,16], and bottle microresonators [17]. However, these theories are not suitable for describing the MI of axial modes. Indeed, the theories for azimuthal modes are derived by assuming equal mode volumes and equal coupling strengths for different azimuthal numbers, a condition that is not satisfied for a series of axial modes.

The first steps toward describing nonlinear interactions between axial modes were made by Oreshnikov and Skryabin [18]. Their work demonstrates the theory of MI of axial modes in a bottle microcavity considering differences in the volume of axial modes. Nevertheless, there is another feature of the SNAP cavities that should be considered [19]. As modes are extended differently along the microcavity axis z, the differences in the overlap integrals of those with a mode of a coupling element become noticeable. As a result, the coupling strength between different modes can differ by an order of magnitude as well as the loaded quality factor. This strongly complicates nonlinear dynamics [19].

Finally, the smallness of the radius variations utilized in a SNAP cavity makes it strongly sensitive to external disturbances. The exciting element, i.e., a taper, has a noticeable influence: In most of the implemented experiments with SNAP cavities, the taper introduces additional effective radius variations [20] and, as a result, an alternating shift of the axial mode frequencies, that is, to additional dispersion [1,19]. Thus, to describe the formation of the primary axial comb in a SNAP resonator, a more complete model is demanded.

*a.kolesnikova@g.nsu.ru

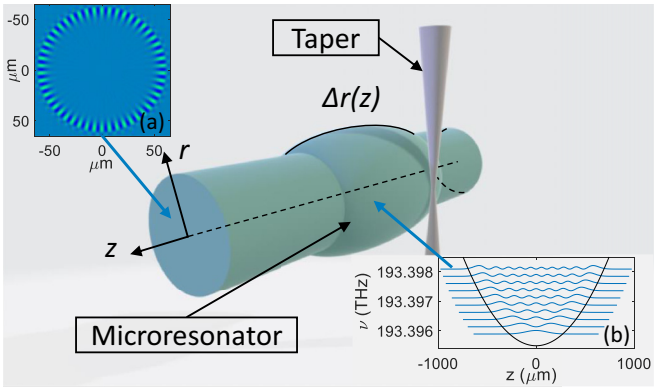

FIG. 1. Surface nanoscale axial photonics (SNAP) system: Microresonator based on the standard optical fiber with an effective radius variation coupled with an input/output taper. Insertions are the spatial distribution of microcavity modes. (a) Azimuthal-radial mode with $m = 50$ and $p = 1$ in the cross-section of the fiber with radius $r_0 = 62.5\,\mu$m. (b) Axial modes with $q = 0, \ldots, 9$ in a microcavity with a parabolic radius variation along the z axis; the resonant frequencies of axial modes are on the ordinate axis.

In this paper, we propose a theory of MI of axial-azimuthal modes, which includes the dependence of mode volume and coupling strength on the axial mode number. Within the framework of the theory, a relation between the power threshold for the nonlinear generation of modes and mode dispersion has been found. Importantly, the derived model relies on the experimentally observable parameters, thus predicting the actual thresholds and paving the way to ease the experimental achievement of the nonlinear generation in SNAP cavities.

In Sec. II, we introduce a system of coupled equations describing the nonlinear dynamics of axial-azimuthal modes with external continuous-wave pumping. Section III describes the nonlinear amplitude-frequency response of the strongly pumped mode. Section IV presents the theory of MI of two sidebands with the detailed derivation in Appendix and separately discusses the generation of azimuthal and axial primary combs since the nature of generation is fundamentally different.

II. SYSTEM OF COUPLED MODE EQUATIONS

To obtain a system of coupled equations for axial-azimuthal modes, we use the representation of the electric field as follows:

$$E(\vec{r}, t) = \sum_{\mu} a_{\mu}(t) e_{\mu}(\vec{r}) \exp(i\omega_s t) + \text{c.c.} \tag{1}$$

Here, $e_{\mu}(\vec{r}) = e_{m,p}(r, \varphi) Z_q(z)$ is the spatial distribution of a mode with azimuthal number m and axial number q, such that $\max |e_{\mu}(\vec{r})| = 1$. Also, $e_{m,p}(r, \varphi)$ is defined by the Bessel function, with the exact expression given in Ref. [21]. Hereinafter, only one radial mode will be considered with the radial quantum number $p = 1$.

Further, $Z_q(z)$ is the spatial distribution of an axial mode, which depends on the form of a fiber radius variation, ω_s is the frequency of the source. In the following, we replace the indexes (m, q) by one index $\mu = (m - m_0, q - q_0) \equiv (m_{\mu}, q_{\mu})$, which is the side mode number, defined concerning a pumped mode with m_0 and q_0.

Using the representation in Eq. (1), from Maxwell's equations, and following the derivations [19], we obtained a system of coupled modes:

$$i\frac{\partial a_{\mu}(t)}{\partial t} - \Delta\omega_{\mu} a_{\mu}(t) + i\delta_{\mu}(z_0) a_{\mu}(t) - \frac{3\omega_{\mu}\chi^{(3)}}{2K_m n_m^2 V_{\mu}} F_{\mu}(\vec{A}) = \delta_{\mu\mu_0} \sqrt{\frac{P_{in}\delta_{c_{\mu}}(z_0)}{\varepsilon_0 n_m^2 V_{\mu}}}. \tag{2}$$

Here, z_0 is the point of the taper position, $\delta_{c_{\mu}}(z_0) = |C_m|^2 Z_q^2(z_0)/L_q$ is the decrement that determines coupling between the mode of the exciting element (taper) and the microresonator mode, $\delta_{\mu}(z_0) = \text{Im}(D_m) Z_q^2(z_0)/L_q + \Gamma$ is the decrement, including the internal losses of the microresonator Γ and taper-induced losses that depend on the overlapping of all radiative modes of the taper with the cavity mode, D_m and C_m are the coupling parameters [19], $L_q = \int Z_q^2(z) dz$ is the effective mode length, $V_{\mu} = L_q \int |e_m(r, \varphi)|^2 d^2 r$ is the effective mode volume. and $\delta_{\mu\mu_0}$ is the Kronecker delta.

Here, $\chi^{(3)}$ is the nonlinear susceptibility, ε_0 is the vacuum permittivity, $K_m = 1 + \frac{\omega_m^{(az)}}{n_m} \frac{\partial n}{\partial \omega}[\omega_m^{(az)}]$ is the coefficient of material dispersion, $n_m \equiv n[\omega_m^{(az)}]$ is the refractive index, and $\omega_m^{(az)}$ is the resonance frequency of azimuthal mode m in the case of infinite cylinder.

Moreover, $\Delta\omega_{\mu} = \omega_p - \omega_{\mu} - \Omega_{\mu}(z_0)$ is the pump frequency detuning from the axial-azimuthal resonant frequency ω_{μ}, $\Omega_{\mu}(z_0) = \text{Re}(D_m) Z_q^2(z_0)/L_q$ is the resonant frequency offset associated with the taper, which introduces additional radius variation as a result of the mode shifts. Also, P_{in} is the pump power. The nonlinear term is determined as

$$F_i(\vec{A}) = \left(V_{iiii}|a_i|^2 + 2\sum_{j \neq i} V_{jjii}|a_j|^2 \right) a_i + \sum_{\substack{j \neq i \\ k \neq i}} V_{ijkl} a_j a_k a_l^*. \tag{3}$$

Here, $V_{ijkl} = \int e_i^*(\vec{r}) e_j(\vec{r}) e_k(\vec{r}) e_l^*(\vec{r}) d^3 r$ is the overlap integral of modes involved in four-wave mixing.

III. PUMPED MODE EQUATION

This is the equation for the central mode with pumping and quantum numbers m_0 and q_0:

$$i\frac{\partial a_0}{\partial t} - \Delta\omega_0 a_0 + i\delta_0 a_0 - g_0 |a_0|^2 a_0 = F. \tag{4}$$

Here, the coefficient of nonlinearity is $g_0 = \frac{3\omega_0 \chi^{(3)} V_{0000}}{2K_{m_0} n_{m_0}^2 V_0}$, $F = \sqrt{\frac{P_{in}\delta_c}{\varepsilon_0 n_{m_0}^2 V_0}}$. In the stationary case, after multiplying Eq. (4) by the complex conjugate, we get

$$F^2 = g_0^2 A^3 + 2g_0 \Delta\omega_0 A^2 + (\delta_0^2 + \Delta\omega_0^2) A. \tag{5}$$

Here, $A = |a_0|^2$. This equation defines the nonlinear frequency response (NFR) of the pumped central mode:

$$\Delta\omega = -g_0 A \pm \sqrt{\frac{F^2}{A} - \delta_0^2}. \tag{6}$$

This expression coincides with the theory of a simple coupling model [22] except for the nonlinearity coefficients g_0. In this case, the frequency is the resonant frequency of the azimuthal mode, and there is a correction factor K_m associated with the material dispersion.

The presence of two branches leads to the bistability of the system [9]. The stable state of the central mode is the upper branch of the NFR with a plus sign in Eq. (6).

IV. PRIMARY COMB GENERATION

To find the pump power that is sufficient to induce primary comb generation, let us consider a pair of modes with $\pm\mu = \pm(m - m_0, q - q_0)$ in the presence of the strongly pumped mode. Linearization of the system of Eq. (2) for sideband modes yields

$$\begin{aligned}
&\frac{\partial a_\mu}{\partial t} + i\Delta\omega_\mu a_\mu + \delta_\mu a_\mu + i2g_{\mu,\mu}|a_0|^2 a_\mu + ig_{\mu,-\mu}a_0^2 a_{-\mu}^* = 0,\\
&\frac{\partial a_{-\mu}^*}{\partial t} - i\Delta\omega_{-\mu}a_{-\mu}^* + \delta_{-\mu}a_{-\mu}^* - i2g_{-\mu,-\mu}|a_0|^2 a_{-\mu}^* - ig_{-\mu,\mu}a_0^{*2}a_\mu = 0.
\end{aligned} \tag{7}$$

Here, $g_{i,j} = \frac{3\omega_i \chi^{(3)} V_{ij00}}{2K_{m_i} n_{m_i}^2 V_i}$, where $i, j \in (-\mu, \mu)$. Further, we use $g_{\pm\mu,\pm\mu} \equiv g_{\pm\mu}$.

The generation of the first pair of modes will start when the amplitude a_0 of the pumped mode is sufficiently large to ensure the instability of the system of linear differential equations [9]. In other words, a part of the NFR must lie inside the region of instability. A detailed derivation of the boundaries of the instability region is given in Appendix. As a result, we obtain

$$\begin{aligned}
\Delta\omega_0 = &-(g_\mu + g_{-\mu})A + \frac{D_\mu^{(\mathrm{int})} + D_{-\mu}^{(\mathrm{int})}}{2}\\
&\pm\sqrt{\frac{(\delta_\mu + \delta_{-\mu})^2}{4\delta_\mu\delta_{-\mu}}(g_{\mu,-\mu}g_{-\mu,\mu}A^2 - \delta_\mu\delta_{-\mu})}.
\end{aligned} \tag{8}$$

Here, $D_{\pm\mu}^{(\mathrm{int})}$ is the mode dispersion term, determined as $\omega_{\pm\mu} = \omega_0 \pm D_1\mu + D_2\mu^2 + \ldots = \omega_0 \pm D_1\mu + D_{\pm\mu}^{(\mathrm{int})}$, including the additional dispersion from the taper.

The pump power $P_{in}^{(th)}$ required for nonlinear generation is determined by the situation when the maximum amplitude $|a_0|^2 = F^2/\delta_0^2$, which is achievable at the given P_{in}, reaches the minimum amplitude required for the MI of the modes, which is defined by the positive sign of the radicand in Eq. (8): $|a_0|^2 = \sqrt{\delta_\mu\delta_{-\mu}/(g_{\mu,-\mu}g_{-\mu,\mu})}$.

Then the minimal power threshold reads

$$P_{in}^{(th)} \geqslant \frac{\delta_0^2\varepsilon_0 n_0^2 V_0}{\delta_c}\sqrt{\frac{\delta_\mu\delta_{-\mu}}{g_{\mu,-\mu}g_{-\mu,\mu}}}. \tag{9}$$

Note that the condition in Eq. (9) is necessary but not sufficient. To determine the real threshold, one needs to consider the position of the boundaries of the instability region relative to the NFR and to demand their not-empty intersection. This consistency condition for Eqs. (6) and (9) might be solved graphically.

A. Azimuthal modes

To more clearly emphasize the features of the nonlinear generation of axial modes, let us first consider the classical case of azimuthal modes with the same axial quantum number, like the nonlinear generation in other microcavities such as microspheres, ring microcavities, with the detailed analysis presented in Ref. [9].

In this case, we can neglect the difference between decrements and the effective volume of different modes; thus, the power threshold becomes independent of the sideband number μ:

$$P_{in}^{(th)} = \frac{\delta_0^3\varepsilon_0 n_0^2 V_0}{\delta_c g_0}. \tag{10}$$

The boundary of the instability region in Eq. (8) is correspondingly simplified to the following form [9]:

$$\Delta\omega_0 = -2g_0 A + \frac{D_\mu^{(\mathrm{int})} + D_{-\mu}^{(\mathrm{int})}}{2} \pm \sqrt{g_0^2 A^2 - \delta_0^2}. \tag{11}$$

We illustrate the rather tolerant requirements for the dispersion for the generation of the azimuthal mode by analyzing the instability region and NFR on the $(\Delta\nu; A)$ plot. To determine azimuthal dispersion in SNAP cavities $D_\mu^{(\mathrm{int})}$, we use the approximation formula for resonant frequencies of the modes of infinite cylinders [21], considering material dispersion of silica (see Fig. 2). Note that, corresponding to Eq. (11), the shape of the boundary does not depend on the sideband number μ. Growing of the dispersion shifts the boundary along the $\Delta\nu$

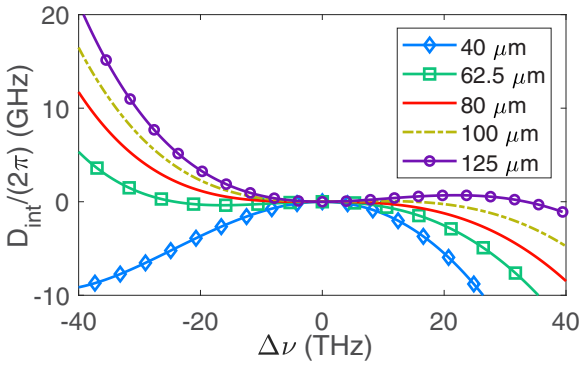

FIG. 2. Dispersion of the azimuthal modes for the various radii of the fiber; $\Delta\nu = \Delta\omega_0/(2\pi)$ is frequency detuning from 193 THz.

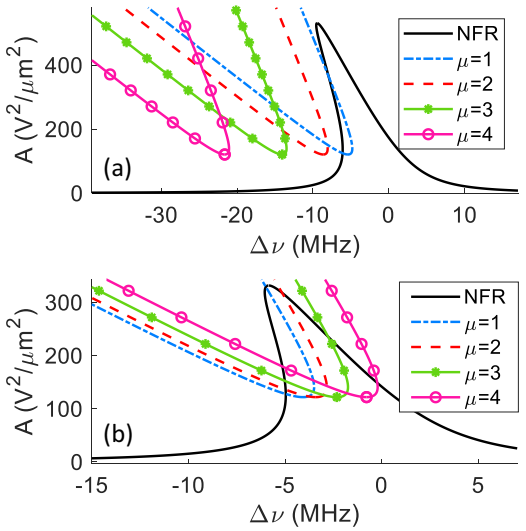

FIG. 3. The instability regions for azimuthal sidebands with number $\mu = 1$–4, and the nonlinear frequency response (NFR) of a mode pumped with $P_{in} = 1$W for different cylinder radii: (a) $r_0 = 62.5\,\mu$m, $m = 354$ (normal dispersion, generation is impossible) and (b) $r_0 = 200\,\mu$m, $m = 1152$ (anomalous dispersion, generation is possible).

axis only (see Fig. 3, the instability region lies inside the hyperbolalike branches). Accordingly, the number of modes that can be potentially involved in degenerate four-wave mixing is determined only by the dispersion value. Negative dispersion yields no intersection between the NFR and instability region [Fig. 3(a)] and thus prohibits the generation, while positive dispersion, which is realized for silica fibers with a radius $>80\,\mu$m, ensures the intersection between the instability region boundary and the NFR. As an example, we considered commercially available fiber with a radius $r_0 = 200\,\mu$m [Fig. 3(b)]. Notably, there are many sidebands that can be generated.

It is also worth noting that, for an arbitrary low level of positive dispersion, the stable branch of the NFR partly falls into the instability region for some sidebands. That is, an arbitrarily small positive dispersion is sufficient for nonlinear generation.

B. Axial modes

The primary comb generation of axial modes with the same azimuthal number appears to be a more intricate process with additional constraints. The modes with different axial numbers q possess different effective volumes ($g_\mu \neq g_{-\mu} \neq g_0$) that cannot be neglected in the analysis. The second important feature is that different axial modes have different overlap integrals with the radiation source, which leads to different coupling strengths and thus loaded quality factors of the modes at the same taper position ($\delta_\mu \neq \delta_{-\mu} \neq \delta_0$).

Foremost, inequalities of g_μ, δ_μ make the nonlinear generation threshold in Eq. (9) dependent on mode number μ, which is a fundamental distinction from the generation of azimuthal modes. As the value of μ increases, the power threshold also increases.

As an illustration, we analyze the threshold power for axial modes, appearing in the fiber with the radius of $r_0 =$

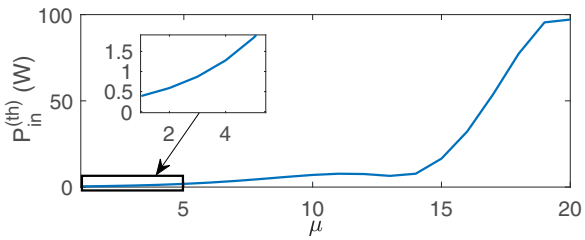

FIG. 4. Power threshold for nonlinear generation of axial modes depending on the sideband number μ.

62.5 μm with considerable parabolic effective radius variation $\Delta r^{(\mathrm{eff})} = \delta r[1 - (z/l)^2]$, where $\delta r = 7$ nm and $l = 2000\,\mu$m. Such variation dimensions are practically achievable, for instance, with strong bending of an optical fiber [4], and should contain ∼100 axial modes, thus being attractive for low-repetition rate optical frequency comb generation. We assume pumping the mode with quantum numbers $m = 354$, $q = 45$ corresponding to the wavelength 1.55 μm. The coupling parameters correspond to the parameters measured in Ref. [19] and have the following values: $\mathrm{Im}(D_m) = 8 \times 10^4$ m/s, $\mathrm{Re}(D_m) = -10^5$ m/s, $|C_m|^2 = 2 \times 10^4$ m/s, and internal losses $\Gamma = 9 \times 10^6\,\mathrm{s}^{-1}$. The minimum threshold for the nonlinear generation with the coupling parameters selected from Ref. [19] is $P_{th}^{(\min)} = 0.4$ W for $\mu = 1$ (see Fig. 4). It is noteworthy that such a high threshold is attributed to the moderate efficiency of the not-single-mode taper used in the experiments [19].

At the given pump power, only the pairs of modes closest to the pump are allowed for generation. For instance, in the case of pumping with power $P_{in} = 1$ W, it is fundamentally possible to generate only sidebands with numbers $\mu = 1, 2, 3$ [see Fig. 5(a)]. Modes with a higher number do not become unstable with such pump power [instability regions for $\mu \geqslant 4$ lay above the NFR curve, see Fig. 5(a)]. This is in contrast with azimuthal modes, which have instability regions located at the same pump level (see Fig. 3).

Importantly, to achieve primary comb generation, a certain dispersion value is required. With increasing number μ, the instability region shifts to the negative detunings even in the absence of the dispersion [see Fig. 5(a)]. Therefore, the presence of anomalous dispersion itself does not guarantee sideband MI, as it did for azimuthal modes. To move the instability regions to the right and ensure their intersection with the NFR curve and thus MI, it is necessary to create an anomalous dispersion of sufficient magnitude.

We obtain dispersion for nonlinear generation at a minimum threshold in Eq. (9) achieved for sideband with $\mu = 1$. At this power, the maximum frequency response is $A = \sqrt{\delta_1\delta_{-1}/(g_{1,-1}g_{-1,1})}$ when $\Delta\nu = -g_0 A$. For MI, the frequency response and the instability region must intersect at this maximum point of NFR; that is, in addition to the amplitudes, the detuning $\Delta\nu$ must be equal: $-g_0 A = -(g_1 + g_{-1})A + D_2$. From this condition, we obtain an expression for the necessary level of the second-order dispersion:

$$D_2^{(th)} = (g_1 + g_{-1} - g_0)\sqrt{\frac{\delta_1\delta_{-1}}{g_{1,-1}g_{-1,1}}}. \qquad (12)$$

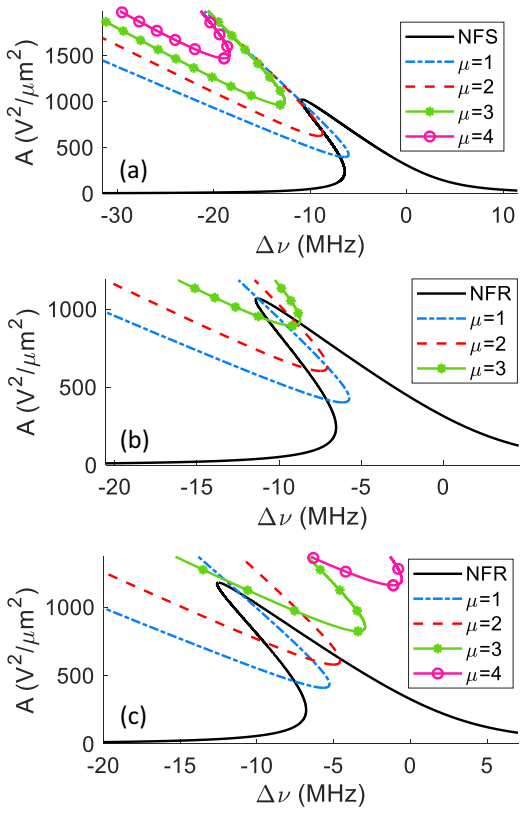

FIG. 5. Instability regions of axial sidebands with number $\mu = 1$–4 relative to the nonlinear frequency response (NFR) at pump power $P_{in} = 1$W with dispersion of axial mode determined by anharmonic term to parabolic potential: (a) No anharmonicity $[D_2/(2\pi) = 0\,\text{MHz}]$, (b) $\alpha = 0.48$ $[D_2/(2\pi) = 0.5\,\text{MHz}]$, and (c) $\alpha = 2.4$ $[D_2/(2\pi) = 2.5\,\text{MHz}]$.

For the potential considered here with $\delta r = 7\,\text{nm}$ and $l = 2000\,\mu\text{m}$, Eq. (12) gives a dispersion $D_2^{(th)}/(2\pi) = 2.15\,\text{MHz}$. In a parabolic potential, the energy levels are equally spaced, yielding $D_2 = 0$. Axial mode dispersion can be introduced by adding anharmonicity to the parabola. Thus, the anharmonic term proportional to z^4 leads to second-order dispersion in the first order of perturbation theory [23]. The value given here is an estimate since introducing dispersion into the parabolic potential will change the distribution functions of the axial modes, so several iterations are necessary to accurately calculate the actual value.

The threshold dispersion depends on the strength of the coupling between the taper and the microcavity and can be further reduced for the undercoupling regime. It is possible to estimate the minimum threshold dispersion, assuming that the microcavity is unloaded. The estimation gives $D_2^{(th)} = 1.43\,\text{MHz}$, i.e., of the same order with the threshold dispersion for the well-loaded quality.

Moreover, by selecting the dispersion, it is possible to select the modes involved in the generation. To illustrate this, we performed calculations for the instability region for axial modes with small second-order dispersion. For this, an anharmonic distortion was added to the parabolic potential

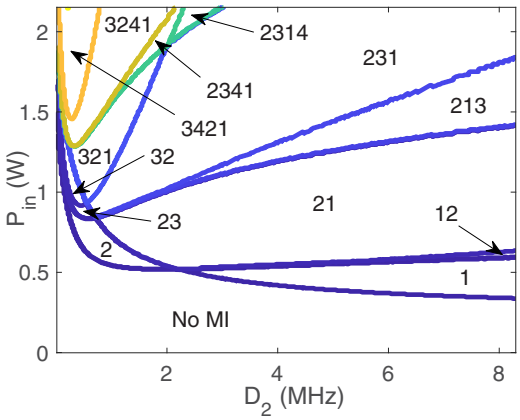

FIG. 6. Modulation instability (MI) map for axial modes. The sequence of numbers corresponds to the order in which side modes μ are involved into the process of degenerate four-wave mixing as the pump frequency decreases.

determined by the shape of an effective radius variation:

$$V_m(z) = 2\beta_m^2 \frac{\delta r}{r_0}\left[1 - \left(\frac{z}{l}\right)^2 + \alpha\left(\frac{z}{l}\right)^4 - \alpha\right]. \qquad (13)$$

Here, α is the anharmonicity coefficient, defining the second-order dispersion D_2 of the axial modes: $\alpha = D_2\omega_m^{(az)} n_m^2 K_m l^2/(3c^2)$ [1,5,23]. Anharmonicity also leads to a change in the axial mode distribution functions and therefore their volumes, which results in a weak dependence of the NFR on dispersion (see Fig. 5).

In the case of low dispersion of $D_2/(2\pi) = 0.5\,\text{MHz}$, regions with $\mu = 2, 3$ do intersect the upper branch of the NFR [see Fig. 5(b)]. With the larger dispersion $D_2/(2\pi) = 2.5\,\text{MHz}$, generation of a mode with $\mu = 3$ becomes impossible; at the same time, closer sidebands $\mu = 1, 2$ meet the generation requirements [see Fig. 5(c)]. Importantly, increasing dispersion results in lower thresholds for the nonlinear generation: The generation of the sideband $\mu = 2$ is available at a lower amplitude of the pump mode $A = 640\,\text{V}^2/\mu\text{m}^2$ than $A = 950\,\text{V}^2/\mu\text{m}^2$ at $D_2/(2\pi) = 0.5\,\text{MHz}$. If we stop the frequency tuning, for example, at $\Delta\nu = -6\,\text{MHz}$, only $\mu = 2$ will be generated. Then as a result of nondegenerate four-wave mixing, only every second mode will appear.

The analysis may be generalized on the instability map (see Fig. 6). The map in the $(D_2; P_{in})$ space indicates the region where MI may occur. This region is subdivided into distinct areas based on which particular modes are amplified under the specified D_2 and P_{in} parameters. Note that different sidebands appear at different detunings of the pump frequency when it is scanned toward the long-wavelength wing of the nonlinear resonance of the pump modes. Thus, we can indicate specific sequences of sideband numbers in the order in which they appear as the pump frequency decreases.

Figure 6 highlights the potential for mode selection during the primary comb formation. For instance, at a pump power of 1 W and a dispersion of 6 MHz, MI can give rise to $\mu = 2$ sidebands at a specific detuning, while the appearance of $\mu = 1$ sidebands occurs with a greater redshift of the pump. At the same time. adjusting dispersion to a smaller value of 0.5 MHz

helps in altering the primary comb formation: The same pump power induces the $\mu = 3$ sidebands in the first instance.

We suppose that the mode selection in a degenerate process defines the further formation of the comb spectrum. For instance, the MI amplifying the third sideband $\mu = 3$ might bring the spectrum with comb teeth being harmonic to the primary sideband [9], giving rise to combs with multiple FSR spacings [24,25] and leading to multisoliton solutions. We presume that the different mode distributions for different axial modes may suppress the nonlinear four-wave mixing, strengthening this tendency.

V. CONCLUSIONS

We investigate the primary comb generation in a cylindrical microresonator with an effective radius variation. Such a system has two sets of equidistant modes: one with only a different axial number and one with only a different azimuthal number. We provide the MI analysis for axial-azimuthal sidebands and determine the threshold for nonlinear generation.

We reveal that the MI of sidebands with different axial quantum numbers has a fundamental difference compared with the generation of azimuthal modes, which is classical for other types of microresonators used for optical comb generation. Inequalities in mode volumes and coupling strengths for different axial modes increase the nonlinear generation threshold with the sideband number, while for azimuthal modes, it is constant. The minimum power threshold is achieved for the first axial sideband and has a value of 400 mW for the investigated microresonator. The dependence of threshold on sideband number leads to the fact that, for a given pump power, the modes closest to the pump mode are involved in the generation, and the gain spectrum includes only a few modes. However, for azimuthal modes, the gain spectrum can include dozens of modes, and its maximum can be far from the pump.

Importantly, to achieve axial mode nonlinear generation at threshold power, a certain dispersion value is required. In contrast with the case of azimuthal modes, in which an arbitrarily small anomalous mode dispersion is sufficient for generation, the gain of axial modes will not begin with any anomalous dispersion. We obtain the expression of the necessary dispersion for nonlinear generation at a minimum threshold for the first sideband. For the microresonator under consideration, it amounts to 2.15 MHz.

In addition, we have shown that the developed theory helps in determining the dispersion necessary for the selection of modes involved in the formation of the primary comb at a certain pump power.

ACKNOWLEDGMENTS

This paper was supported by the Russian Science Foundation (Grant No. 22-12-20015) and by the Government of the Novosibirsk Region. We express our gratitude to Evgeny Podivilov and Boris Sturman for productive conversations.

APPENDIX: BOUNDARIES OF THE INSTABILITY REGION

Let us find the roots of the characteristic equation for the system of linear equations in Eq. (7):

$$(-i\Delta\omega_\mu - \delta_\mu - i2g_\mu|a_0|^2 - \lambda)(i\Delta\omega_{-\mu} - \delta_{-\mu} + i2g_{-\mu}|a_0|^2 - \lambda) - g_{\mu,-\mu}g_{-\mu,\mu}|a_0|^4 = 0. \tag{A1}$$

The characteristic equation is

$$\begin{aligned}\lambda^2 + 2\lambda\left[\frac{\delta_\mu + \delta_{-\mu}}{2} + i(g_\mu - g_{-\mu})A + \frac{i(\Delta\omega_\mu - \Delta\omega_{-\mu})}{2}\right] + \Delta\omega_\mu\Delta\omega_{-\mu} + \delta_\mu\delta_{-\mu} \\ + 2i(g_\mu\delta_{-\mu} - g_{-\mu}\delta_\mu)A + (4g_\mu g_{-\mu} - g_{\mu,-\mu}g_{-\mu,\mu})A^2 + 2(g_\mu\Delta\omega_{-\mu} + g_{-\mu}\Delta\omega_\mu)A \\ + i(\Delta\omega_\mu\delta_{-\mu} - \Delta\omega_{-\mu}\delta_\mu) = 0.\end{aligned} \tag{A2}$$

The roots of the characteristic equation are defined as

$$\begin{aligned}\lambda = -\frac{\delta_\mu + \delta_{-\mu}}{2} - i(g_\mu - g_{-\mu})A - \frac{i(\Delta\omega_\mu - \Delta\omega_{-\mu})}{2} \\ \pm\left\{-\frac{(\Delta\omega_\mu + \Delta\omega_{-\mu})^2}{4} + \frac{(\delta_\mu - \delta_{-\mu})^2}{4} - (g_\mu + g_{-\mu})^2A^2 - (\Delta\omega_\mu + \Delta\omega_{-\mu})(g_\mu + g_{-\mu})A\right. \\ \left. - g_{\mu,-\mu}g_{-\mu,\mu}A^2 + i\big(\delta_\mu - \delta_{-\mu}\big)\left[(g_\mu + g_{-\mu})A + \frac{\Delta\omega_\mu + \Delta\omega_{-\mu}}{2}\right]\right\}^{1/2}.\end{aligned} \tag{A3}$$

The instability condition is $\mathrm{Re}\,\lambda > 0$:

$$\mathrm{Re}\,\lambda = -\frac{\delta_\mu + \delta_{-\mu}}{2} \pm \mathrm{Re}\,\sqrt{\zeta}. \tag{A4}$$

Here, $\zeta = -(\Delta\omega_\mu + \Delta\omega_{-\mu})^2/4 + (\delta_\mu - \delta_{-\mu})^2/4 - (\Delta\omega_\mu + \Delta\omega_{-\mu})(g_\mu + g_{-\mu})A - [(g_\mu + g_{-\mu})^2 - g_{\mu,-\mu}g_{-\mu,\mu}]A^2 + i(\delta_\mu - \delta_{-\mu})[(g_\mu + g_{-\mu})A + (\Delta\omega_\mu + \Delta\omega_{-\mu})/2]$.

Considering that $\mathrm{Re}(\sqrt{\zeta}) = \pm\sqrt{[|\zeta| + \mathrm{Re}(\zeta)]/2}$, we obtain the condition for the onset of instability:

$$\frac{(\delta_\mu + \delta_{-\mu})^4}{4} - (\delta_\mu + \delta_{-\mu})^2\,\mathrm{Re}(\zeta) - \mathrm{Im}(\zeta)^2 < 0. \tag{A5}$$

We introduce the notation: $\delta^+ = (\delta_\mu + \delta_{-\mu})/2$, $\delta^- = (\delta_\mu - \delta_{-\mu})/2$, $\Delta\omega^+ = (\Delta\omega_\mu + \Delta\omega_{-\mu})/2$, $g = g_\mu + g_{-\mu}$, and $g^{(2)} = g_{\mu,-\mu}g_{-\mu,\mu}$. In this case, $\mathrm{Re}(\zeta) = -(\Delta\omega^+)^2 + (\delta^-)^2 - 2\Delta\omega^+ gA - [g^2 - g^{(2)}]A^2$, $\mathrm{Im}(\zeta) = 2\delta^-(gA + \Delta\omega^+)$:

$$(\delta^+)^4 - (\delta^+)^2\{-(\Delta\omega^+)^2 + (\delta^-)^2 - 2\Delta\omega^+ gA - [g^2 - g^{(2)}]A^2\} - [\delta^-(gA + \Delta\omega^+)]^2 < 0. \tag{A6}$$

Now it is necessary to find the boundaries of the instability region expressed in terms of the parameters $\Delta\omega_0$ and A, considering $\Delta\omega^+ = \Delta\omega_0 + [2\omega_0 - \omega_\mu - \omega_{-\mu} - (2\Omega_0 - \Omega_\mu - \Omega_{-\mu})]/2 = \Delta\omega_0 - [D_\mu^{(\mathrm{int})} + D_{-\mu}^{(\mathrm{int})}]/2$. Let us denote $D^+ = [D_\mu^{(\mathrm{int})} + D_{-\mu}^{(\mathrm{int})}]/2$. Thus, we obtain the quadratic equation for $\Delta\omega_0$:

$$\begin{aligned}&[(\delta^+)^2 - (\delta^-)^2]\Delta\omega_0^2 + 2[(\delta^+)^2 - (\delta^-)^2](gA - D^+)\Delta\omega_0 + [(\delta^+)^2 - (\delta^-)^2](gA - D^+)^2 \\ &\quad - (\delta^+)^2[(\delta^-)^2 + g^{(2)}A^2] + (\delta^+)^4 = 0.\end{aligned} \tag{A7}$$

The discriminant of the quadratic equation is

$$\begin{aligned}D &= [(\delta^+)^2 - (\delta^-)^2]\{(\delta^+)^2[(\delta^-)^2 + g^{(2)}A^2] - (\delta^+)^4\} \\ &= (\delta^+)^2[(\delta^+)^2 - (\delta^-)^2][(\delta^-)^2 + g^{(2)}A^2 - (\delta^+)^2].\end{aligned} \tag{A8}$$

The boundaries of the stability region are

$$\Delta\omega_0 = -gA + D^+ \pm \sqrt{\frac{(\delta^+)^2[(\delta^-)^2 + g^{(2)}A^2 - (\delta^+)^2]}{(\delta^+)^2 - (\delta^-)^2}}, \tag{A9}$$

when we go back to the previous notation and obtain Eq. (8).

[1] M. Sumetsky and J. M. Fini, Surface nanoscale axial photonics, Opt. Express **19**, 26470 (2011).

[2] M. Sumetsky, Nanophotonics of optical fibers, Nanophotonics **2**, 393 (2013).

[3] V. Dvoyrin and M. Sumetsky, Bottle microresonator broadband and low-repetition-rate frequency comb generator, Opt. Lett. **41**, 5547 (2016).

[4] D. Bochek, N. Toropov, I. Vatnik, D. Churkin, and M. Sumetsky, SNAP microresonators introduced by strong bending of optical fibers, Opt. Lett. **44**, 3218 (2019).

[5] S. V. Suchkov, M. Sumetsky, and A. A. Sukhorukov, Frequency comb generation in SNAP bottle resonators, Opt. Lett. **42**, 2149 (2017).

[6] A. A. Savchenkov, A. B. Matsko, D. Strekalov, M. Mohageg, V. S. Ilchenko, and L. Maleki, Low threshold optical oscillations in a whispering gallery mode CaF_2 resonator, Phys. Rev. Lett. **93**, 243905 (2004).

[7] A. B. Matsko, A. A. Savchenkov, D. Strekalov, V. S. Ilchenko, and L. Maleki, Optical hyperparametric oscillations in a whispering-gallery-mode resonator: Threshold and phase diffusion, Phys. Rev. A **71**, 033804 (2005).

[8] T. Herr, K. Hartinger, J. Riemensberger, C. Y. Wang, E. Gavartin, R. Holzwarth, M. L. Gorodetsky, and T. J. Kippenberg, Universal formation dynamics and noise of Kerr-frequency combs in microresonators, Nat. Photon. **6**, 480 (2012).

[9] Y. K. Chembo and N. Yu, Modal expansion approach to optical-frequency-comb generation with monolithic whispering-gallery-mode resonators, Phys. Rev. A **82**, 033801 (2010).

[10] Y. K. Chembo, D. V. Strekalov, and N. Yu, Spectrum and dynamics of optical frequency combs generated with monolithic whispering gallery mode resonators, Phys. Rev. Lett. **104**, 103902 (2010).

[11] T. Hansson, D. Modotto, and S. Wabnitz, Dynamics of the modulational instability in microresonator frequency combs, Phys. Rev. A **88**, 023819 (2013).

[12] D. J. Wilson, K. Schneider, S. Hönl, M. Anderson, Y. Baumgartner, L. Czornomaz, T. J. Kippenberg, and P. Seidler, Integrated gallium phosphide nonlinear photonics, Nat. Photon. **14**, 57 (2020).

[13] T. Herr, V. Brasch, J. D. Jost, C. Y. Wang, N. M. Kondratiev, M. L. Gorodetsky, and T. J. Kippenberg, Temporal solitons in optical microresonators, Nat. Photon. **8**, 145 (2014).

[14] V. Brasch, M. Geiselmann, T. Herr, G. Lihachev, M. H. Pfeiffer, M. L. Gorodetsky, and T. J. Kippenberg, Photonic chip–based optical frequency comb using soliton Cherenkov radiation, Science **351**, 357 (2015).

[15] N. M. Kondratiev and V. E. Lobanov, Modulational instability and frequency combs in whispering-gallery-mode microresonators with backscattering, Phys. Rev. A **101**, 013816 (2020).

[16] N. M. Kondratiev, V. E. Lobanov, E. A. Lonshakov, N. Y. Dmitriev, A. S. Voloshin, and I. A. Bilenko, Numerical study of solitonic pulse generation in the self-injection locking regime at normal and anomalous group velocity dispersion, Opt. Express **28**, 38892 (2020).

[17] Y. V. Kartashov, M. L. Gorodetsky, A. Kudlinski, and D. V. Skryabin, Two-dimensional nonlinear modes and frequency combs in bottle microresonators, Opt. Lett. **43**, 2680 (2018).

[18] I. Oreshnikov and D. V. Skryabin, Multiple nonlinear resonances and frequency combs in bottle microresonators, Opt. Express **25**, 10306 (2017).

[19] A. Y. Kolesnikova and I. D. Vatnik, Theory of nonlinear whispering-gallery-mode dynamics in surface nanoscale axial photonics microresonators, Phys. Rev. A **108**, 033506 (2023).

[20] D. L. P. Vitullo, S. Zaki, D. E. Jones, M. Sumetsky, and M. Brodsky, Coupling between waveguides and microresonators: The local approach, Opt. Express **28**, 25908 (2020).

[21] Y. A. Demchenko and M. L. Gorodetsky, Analytical estimates of eigenfrequencies, dispersion, and field distribution in whispering gallery resonators, J. Opt. Soc. Am. B **30**, 3056 (2013).

[22] M. L. Gorodetsky and V. S. Ilchenko, Optical microsphere resonators: Optimal coupling to high-Q whispering-gallery modes, J. Opt. Soc. Am. B **16**, 147 (1999).

[23] C. M. Bender and T. T. Wu, Anharmonic oscillator. II. A study of perturbation theory in large order, Phys. Rev. D **7**, 1620 (1973).

[24] A. A. Savchenkov, A. B. Matsko, V. S. Ilchenko, I. Solomatine, D. Seidel, and L. Maleki, Tunable optical frequency comb with a crystalline whispering gallery mode resonator, Phys. Rev. Lett. **101**, 093902 (2008).

[25] I. S. Grudinin, N. Yu, and L. Maleki, Generation of optical frequency combs with a CaF_2 resonator, Opt. Lett. **34**, 878 (2009).